

Characterization of low-resistance ohmic contacts to a two-dimensional electron gas in a GaAs/AlGaAs heterostructure

Muhammad Javaid Iqbal^{1,2,*}, Dirk Reuter^{3,**}, Andreas Dirk Wieck³, and Caspar van der Wal¹

¹ Zernike Institute for Advanced Materials, Nijenborgh 4, University of Groningen, NL-9747AG Groningen, The Netherlands

² Centre of Excellence in Solid State Physics, University of the Punjab, QAC, Lahore-54570, Pakistan

³ Angewandte Festkörperphysik, Ruhr-Universität Bochum, D-44780 Bochum, Germany

Received: 25 June 2019 / Received in final form: 11 February 2020 / Accepted: 21 February 2020

Abstract. The study of electron transport in low-dimensional systems is of importance, not only from a fundamental point of view, but also for future electronic and spintronic devices. In this context heterostructures containing a two-dimensional electron gas (2DEG) are a key technology. In particular GaAs/AlGaAs heterostructures, with a 2DEG at typically 100 nm below the surface, are widely studied. In order to explore electron transport in such systems, low-resistance ohmic contacts are required that connect the 2DEG to macroscopic measurement leads at the surface. Here we report on designing and measuring a dedicated device for unraveling the various resistance contributions in such contacts, which include pristine 2DEG series resistance, the 2DEG resistance under a contact, the contact resistance itself, and the influence of pressing a bonding wire onto a contact. We also report here a recipe for contacts with very low resistance values that remain below 10 Ω for annealing times between 20 and 350 s, hence providing the flexibility to use this method for materials with different 2DEG depths. The type of heating, temperature ramp rate and gas forming used for annealing is found to strongly influence the annealing process and hence the quality of the resulting contacts.

1 Introduction

The two-dimensional electron gas (2DEG) is of interest for the study of low-dimensional systems, and high-mobility 2DEGs can be realized in epitaxially grown GaAs/Al_xGa_{1-x}As heterostructures [1,2]. For performing electrical transport experiments on these systems ohmic contacts to the 2DEG are very important, and these can be realized by annealing samples after a metal alloy has been deposited on the surface at the intended contact areas. Commonly, an alloy consisting of AuGe/Ni/Au is used [3]. The AuGe thin film contacts are recently studied and proposed as potential candidates for studying thermoelectric applications on the thin organic layers or molecular junctions as well [4]. The annealing times and temperatures that give the lowest contact-resistance values are different for different 2DEG depths. In our previous work [5,6] we optimized such a recipe for annealing in a glass-tube oven. For the study presented here, we used different annealing conditions, namely annealing in a Rapid Thermal Annealer (RTA). Annealing with the RTA gave low contact resistance values for a very wide range of annealing times at a fixed annealing temperature. These results are attributed to the exact heating profile as a function of time during annealing,

and the process that we followed for cleaning the samples. We already applied our recipes for ohmic contacts in our studies of quantum point contacts on a 2DEG system [7,8].

The AuGe/Ni/Au material was first used by [9] to make an ohmic contact to n-GaAs in 1967. Subsequent studies aimed at improving such contacts and understanding the annealing mechanisms [10–24]. Later on, with the increasing importance of the 2DEG in a GaAs/Al_xGa_{1-x}As heterostructure, research focussed on making ohmic contacts to the buried 2DEG [25–33]. Despite these extensive studies, a model was missing that could predict the optimal annealing times and temperatures for different depths of the 2DEG. In our previous work we developed such a model [5,6]. In order to understand the annealing mechanism further, we studied the contact-resistance values as a function of circumference and area of the ohmic contacts. However, no clear dependence on circumference or area was found [5,6], in part because of lack of information on whether the 2DEG square resistance under an ohmic contact changes during the annealing with respect to the square resistance of pristine 2DEG. In addition, it was unknown whether pressing a bonding wire on a contact influences the resistance, as it can possibly rupture the ohmic contact layer over a significant area. Here we report on studying these questions. We designed a dedicated device structure that allowed us to study the contact resistance with various resistance contributions in more detail, and with different measurement methods (3-point

* e-mail: javid2k@gmail.com

** Present address: Department of Physics, University Paderborn, Warburger Straße 100, D-30098 Paderborn, Germany.

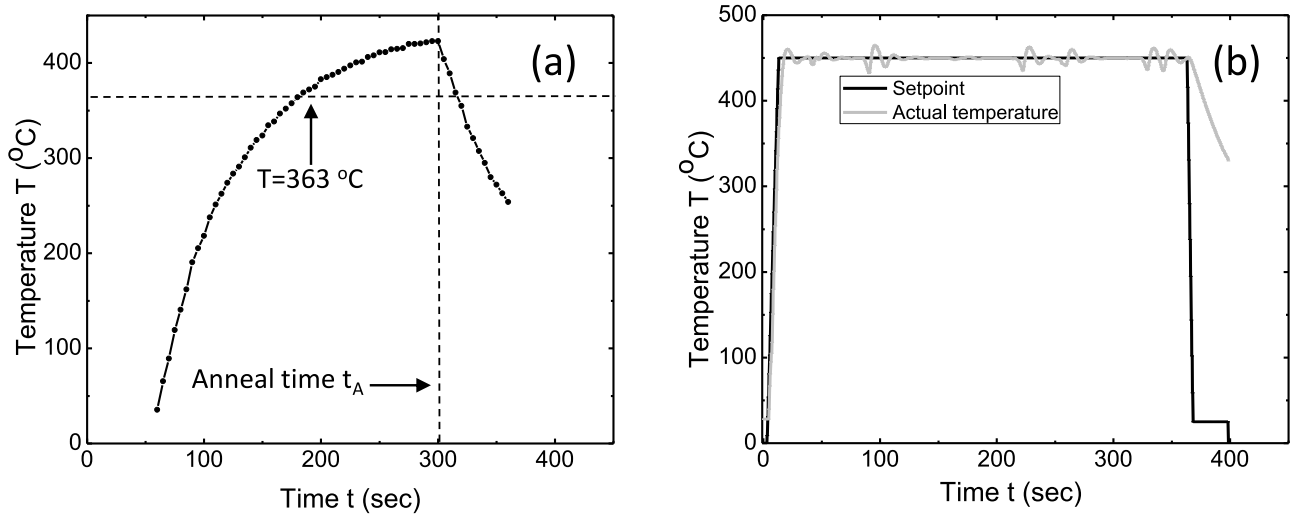


Fig. 1. Temperature of a thermocouple in close contact with the sample as a function of time during the annealing process in the glass-tube furnace (a) and rapid thermal annealer (RTA) (b).

measurement, 4-point measurement and the Transmission Line Method (TLM) [34–36]).

All the results presented in this paper are from samples annealed in a rapid thermal annealer (RTA), unlike our previous work where the hot gas flow in a glass-tube furnace was used for annealing the samples. We used the ultrasonic bonding techniques for all the wires bond in this work as well as in our previous work [5]. In the present study we focused on changes in the mentioned contact resistance contributions as a function of annealing time (at fixed annealing temperature and depth of the 2DEG). Because of the very low resistance values that we have found in all the case for annealing times between 20 and 350s, we could not draw strong conclusions on the contribution and effect of different resistance values. Nevertheless our proposed design could be used to further unravel different resistance contributions in the ohmic contact values. The robust recipe could also be used for annealing to a variety of GaAs/AlGaAs heterostructures with various 2DEG depths.

2 Experimental details

For the present study we used two different wafers, one with the 2DEG at 60 nm depth (wafer I, purchased from Sumitomo Electric Industries, Inc.) and the other with the 2DEG at 180 nm depth (wafer II, grown by our team in Bochum). Unless mentioned otherwise, we present results of devices that were fabricated with wafer I. The study of devices from wafer II were less extensive but we will mention the results that are relevant. All the measurements were performed in a liquid helium vessel at 4.2 K.

Wafer I was a GaAs/Al_{0.27}Ga_{0.73}As heterostructure. The layer sequence of the heterostructure was as follows (top to bottom): a 5 nm *n*-GaAs cap, 40 nm Al_{0.27}Ga_{0.73}As *n*-doped with Si at $2.0 \times 10^{18} \text{ cm}^{-3}$, a 15 nm nominally intrinsic Al_{0.27}Ga_{0.73}As spacer layer, and a 800 nm GaAs layer. The 2DEG is located at the interface

of the AlGaAs spacer layer and the next GaAs layer. The 2DEG density and mobility at 4.2 K were $n_{2D} = 3.30 \times 10^{15} \text{ m}^{-2}$ and $\mu_{2D} = 19.8 \text{ m}^2/\text{Vs}$, respectively. Wafer II was a similar GaAs/Al_{0.35}Ga_{0.65}As heterostructure with the layer sequence (top to bottom): a 5 nm *n*-GaAs cap, 70 nm Al_{0.35}Ga_{0.65}, 70 nm Al_{0.35}Ga_{0.65}As *n*-doped with Si at $\sim 1.0 \times 10^{18} \text{ cm}^{-3}$, 35 nm Al_{0.35}Ga_{0.65}As, and 650 nm GaAs. It had $n_{2D} = 1.93 \times 10^{15} \text{ m}^{-2}$ and $\mu_{2D} = 33.3 \text{ m}^2/\text{Vs}$.

Several cleaning steps during ohmic contact fabrication are very important for getting low-resistance ohmic contacts. The cleaning process is done before starting the ohmic contact fabrication. The samples are first cleaned in acetone, and then in iso-propyl-alcohol, while keeping the sample in an ultrasonic bath on a low power. The samples are then visually inspected and only samples that appear fully clean are used. We observed that contaminated samples show high resistance values and results that cannot be reproduced.

The size of the ohmic contacts was 200 by 200 μm^2 and they were patterned with electron-beam lithography. For the ohmic contacts, layers of AuGe in eutectic-composition (12 wt% Ge, 150 nm), Ni (30 nm) and Au (20 nm) were deposited subsequently by electron-beam evaporation. The contacts were annealed at 450 °C in the rapid thermal annealer (RTA, model Jipelec Jet 150) for various times. Annealing took place in a clean N₂ flow (600 sccm) to avoid oxidation and material vapors adhering back onto the sample. During annealing the functional sample surface was directly facing the RTA heating lamps.

The annealing temperature profiles for the glass-tube oven (used in our previous work [5]) and the RTA are shown in Figures 1a and 1b. For the glass-tube oven, the sample is brought into a pre-heated oven and the temperature rise of the sample holder to the AuGe-eutectic temperature (363 °C) takes a few minutes (not easily controllable). For the RTA, on the other hand, the temperature ramp rate can be controlled and the time for reaching the set temperature was set at the much shorter

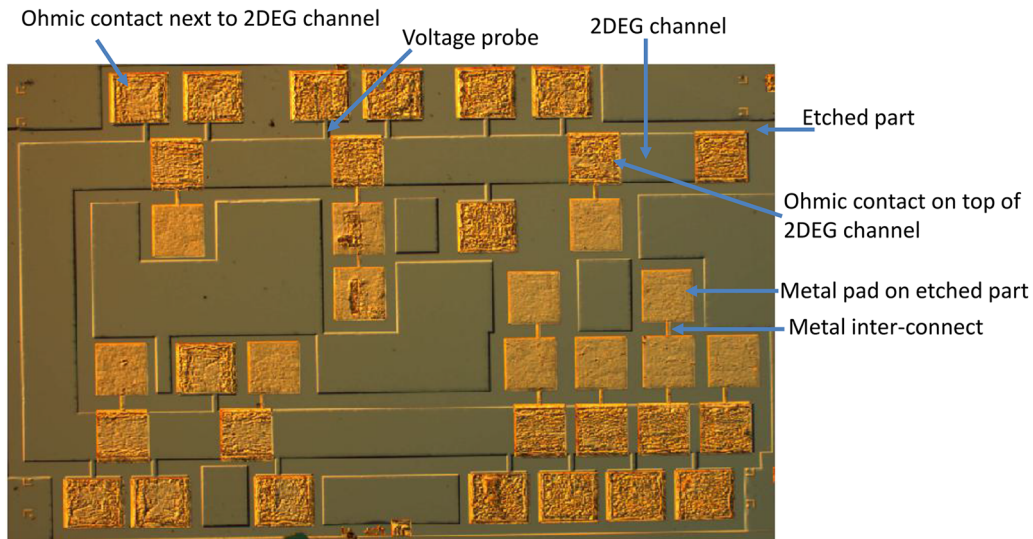


Fig. 2. Optical microscope image of a device showing etched mesa regions and deposited contacts. The shallow part of the mesa is wet-etched at places where the design requires a boundary to a 2DEG region. The ohmic contacts and metal pads (all $200 \times 200 \mu\text{m}^2$) are deposited and annealed on 2DEG and etched surface respectively so that the latter are separated from the 2DEG.

(but for RTA heating typical) value of 5 s. This is started with the sample already in the oven. The black and light gray lines in Figure 1b are for the set temperature and the actual temperature as measured by the thermocouple attached to the surface where sample is placed for annealing. All the results presented in this paper are for samples annealed in the RTA.

The heating sources in the RTA are the halogen lamps that transmit radiation through a quartz window above the sample surface. The sample is placed on a Si base plate and a thermocouple is attached to this plate for measuring the annealing temperature during the process. The flow of N_2 gas is maintained during the entire annealing process and cool down.

3 Device design, measurement schemes and methods

We designed a dedicated device structure for being able to study the different contact-resistance contributions with different measurement methods. An optical image of a fabricated device is shown in Figure 2. A $200 \mu\text{m}$ wide 2DEG channel is defined (U-shaped) by wet etching such that a homogeneous current flow can be applied through the defined strip. Different parts of the devices are labeled. The ohmic contacts are realized on top of the channel as well as on the sides of the channel. The available distances L_i (defined as in Fig. 4a) between the contacts on top of the channel are 40, 260, 460, 660, and $860 \mu\text{m}$. The effect of annealing times on the pristine 2DEG square resistance, on the full contact resistance and 2DEG square resistance under ohmic contacts are determined using the ohmic contacts deposited on top of the 2DEG channel. The ohmic contacts deposited on the sides are connected to the 2DEG channel via narrow 2DEG strips ($20 \mu\text{m}$ wide) and serve as voltage probes (used when measuring the resistance

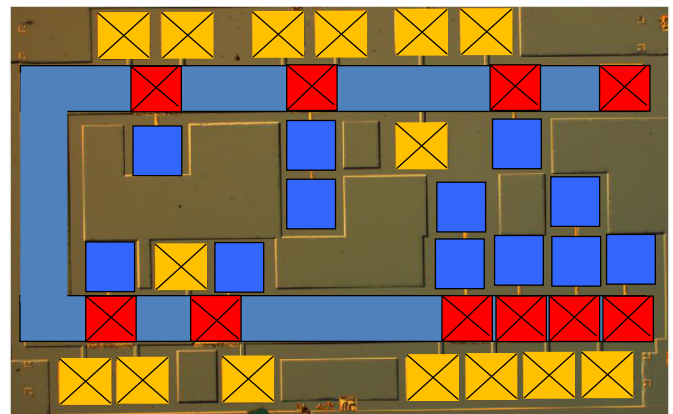


Fig. 3. Color scheme to highlight different parts of the device. The U-shaped blue part is a $200 \mu\text{m}$ wide 2DEG channel. The red squares are ohmic contacts on top of the main 2DEG channel and the yellow squares are ohmic contacts on the side of the channel that only serve as voltage probes. The dark blue squares are metal contact pads on etched wafer areas (all contacts are $200 \times 200 \mu\text{m}^2$).

of the contacts, the resistance of pristine 2DEG and the resistance of 2DEG under contacts). Metal pads and metal inter-connects between pads are deposited on etched parts of the device. These metal pads are connected to the ohmic contacts via metal inter-connects and used for measuring the ohmic contact resistances without directly bonding on the ohmic contacts themselves (the resistance contributions from metal pads and inter-connects are subtracted in this case). By comparing values measured with this bonding scheme to a subsequent measurement with bonding directly on top of the ohmic contacts, the influence of pressing a bonding wire on an ohmic contact can be determined. The color scheme in Figure 3 further illustrates the various device parts more clearly. The long 2DEG channel

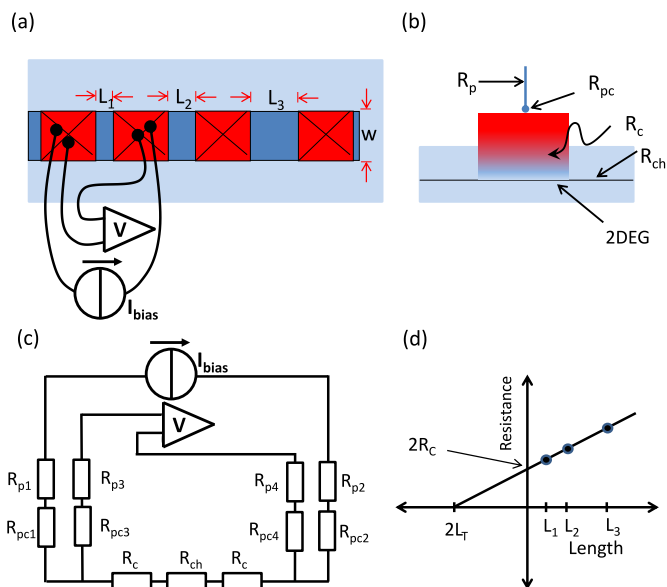


Fig. 4. Transmission Line Method (TLM) measurement scheme. (a) Ohmic contacts are made over the full width of a 2DEG strip with increasing distance L_i between adjacent contacts. A 4-point measurement is used for determining the resistance R_{total} for each segment. (b) A side view on a contact showing the various resistance contributions (see main text for details). (c) A circuit diagram for the 4-point scheme with the resistance contributions from panel (b). (d) A schematic plot of TLM measurement results (see main text for details).

is shown with a light blue color. The ohmic contacts are shown as crossed color squares, with contacts on top of the 2DEG channel in red and side contacts in yellow. The metal pads on etched regions are shown as dark blue squares.

Figures 4 and 5 show the various measurement schemes that we applied in this study. We first explain the Transmission Line Method (TLM) before explaining the other measurement schemes. The TLM method [34–36] is a very accurate method for measuring the values of pristine 2DEG square resistance and ohmic-contact resistance, and is widely used in research on ohmic contacts. Figure 4 shows how the TLM method works. The contacts are made on a 2DEG strip with an increasing distance between pairs of adjacent contacts (Fig. 4a). The width of the contact and channel is labeled as W . For resistance measurements a four point current-biased scheme is used (Fig. 4a). This measurement is carried out for all the consecutive contact pairs. Figure 4b shows a schematic of a side view on one of the contacts and the resistance contributions that play a role. The resistance contributions are R_p (probe resistance), R_{pc} (probe-to-contact resistance), R_c (actual contact resistance between metal pad on the surface and 2DEG) and R_{ch} (2DEG resistance of the channel between the contacts). Figure 4c shows the corresponding circuit diagram for the complete four-probe scheme. Since the probe (R_p) and the probe-to-contact resistances (R_{pc}) are negligible as compared to the input resistance of the voltmeter they can be neglected. The

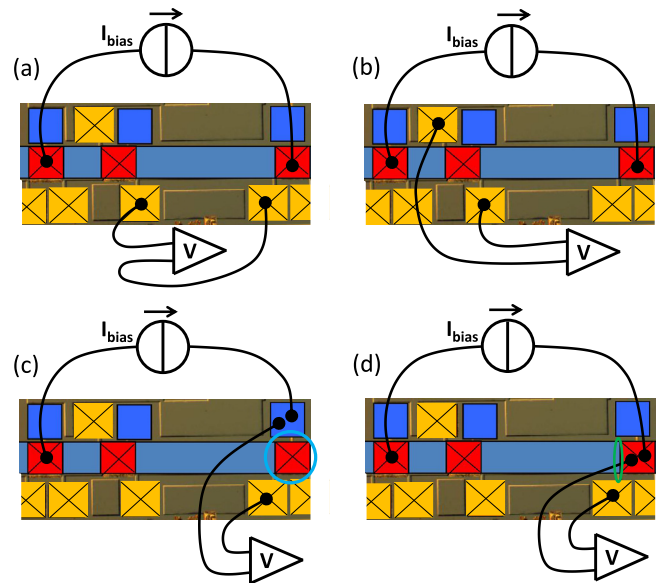


Fig. 5. Various measurement schemes illustrated with colored contacts as in Figure 3. (a) The scheme to measure the pristine 2DEG resistance. (b) The scheme to measure the 2DEG resistance under an ohmic contact. (c) The 3-point measurement scheme for measuring the resistance of an ohmic contact without a bonding wire directly on top of the measured contact (circled in this case). The bonding wire is here on a metal side pad that is connected to the surface metallization of the measured ohmic contact via a narrow metal inter-connect. (d) The 3-point measurement scheme for measuring the resistance of an ohmic contact with bonding directly on top of the measured contact.

total resistance measured between pairs of consecutive contacts is then

$$R_{total} = 2R_c + R_{ch} = V/I, \quad (1)$$

The plot in Figure 4d illustrates how to extract the contact and 2DEG square resistance values from the TLM data. The R_{total} values are plotted as a function of the channel length. The resistance contribution R_{ch} increases linearly with increasing channel length and R_{total} shows a linear dependence with an offset from zero that is equal to $2R_c$. A linear fit to the data points can thus be used to obtain R_c . In addition, the slope of the R_{total} provides an accurate measure for the square resistance R_{\square} of pristine 2DEG (2DEG between contacts). Using that $R_{ch} = R_{\square}L_i/W$ this can be expressed as $R_{\square} = R_{ch}W/L_T$, where the transfer length L_T is defined using the intercept at zero resistance for the linear trend (see Fig. 4d). Our experiment indeed only gave results with a linear dependence of R_{total} on L_i .

We used an extended TLM scheme with first measurements that used bonding on the metal side pads (not shown in Fig. 4) and subsequently measurements that used bonding directly on top of the ohmic contacts (as in Fig. 4) to investigate the influence of pressing a bonding wire on an ohmic contact. Column 6 and 7 in Table 1 show the contact resistance values measured by the TLM method with bonding wires on metal side pads and ohmic

Table 1. The different resistance values for different annealing times. Row 3 list the figures with the corresponding measurement schemes. Column 2 and 3 are for the 2DEG square resistance and 2DEG square resistance under the contacts, respectively. Column 4 and 5 are for the contact resistance measured by the 3-point method with the bonding wires on side pads and the ohmic contacts, respectively. Column 6 and 7 report the contact resistance as determined with the TLM method, with the bonding wires on side pads and the ohmic contacts, respectively.

1	2	3	4	5	6	7
$t_A(\text{sec})$	$R_{\square}(\Omega)$	$R_{\square, \text{below}C}(\Omega)$	$R_{c, 3p\text{-pad}}(\Omega)$	$R_{c, 3p\text{-ohm}}(\Omega)$	$R_{c, \text{TLM-pad}}(\Omega)$	$R_{c, \text{TLM-ohm}}(\Omega)$
–	Figure 5a	Figure 5b	Figure 5c	Figure 5d	Figure 4	Figure 4
20	19.91 ± 1.07	2.25 ± 1.18	8.60 ± 0.75	4.49 ± 0.36	9.18 ± 4.5	0.41 ± 3.4
50	19.61 ± 1.56	3.00 ± 0.30	5.29 ± 1.19	4.00 ± 0.28	6.28 ± 2.86	1.24 ± 1.13
100	19.50 ± 0.60	3.17 ± 1.55	9.04 ± 0.62	4.47 ± 0.45	9.77 ± 0.80	2.38 ± 0.41
350	20.77 ± 0.39	3.78 ± 0.38	7.76 ± 1.02	4.44 ± 0.37	Not measured	2.30 ± 0.30

contacts, respectively. We observe here R_c values that are significantly lower for the case with bonding directly on the ohmic contacts. However, while TLM results give accurate results for R_c , it is not possible to use it conventionally for measuring the 2DEG resistance under an ohmic contact. It also does not give information on where inside a contact the contributions to contact resistance arise, while such information is required for detailed understanding of the annealing mechanism, and understanding the differences between the results in column 6 and 7 in Table 1.

We now discuss other measurement schemes that we applied for determining the various resistance contributions. For a first round of measurements (this order was carried out in parallel with the TLM measurements) bonding wires were pressed on the side ohmic contacts. Two ohmic contacts on top of the 2DEG channel are used for injecting current into the channel (Figs. 5a, 5b). The voltage drop across a known length of pristine 2DEG channel or 2DEG under an ohmic contacts can then be measured with the voltage probes. The measured values R_{\square} (square resistance of pristine 2DEG, no significant deviations from the TLM values) and $R_{\square, \text{below}C}$ (square resistance of 2DEG below an ohmic contact) are shown in column 2 and 3 of the Table 1, respectively.

For a second round of measurements, two bonding wires were pressed onto each metal side pad that connects to the metal layer of an ohmic contact on top of the channel (Fig. 5c). The resistance contributions from the metal side pads and metal inter-connects (measured on each sample, typically 10 Ω) were measured separately and are subtracted. This measurement scheme directly gives values for the total contact resistance of contacts, which are denoted as $R_{c, 3p\text{-pad}}$ and are shown in column 4 of Table 1.

A third round of measurements was carried out as in Figure 5d. This scheme gives directly a value for the total contact resistance of contacts with the bonding wires pressed directly on top of the contact that is measured. The results are denoted as $R_{c, 3p\text{-ohm}}$ and are shown in column 5 of Table 1. We used ultrasonic bonding technique for all the wire bonds in this work.

All the resistance values measured with various schemes are thus collected in Table 1 for different annealing times. The reported values are average of (in most cases) 5 contacts. The reported error margins for column 2 to 5 are the standard deviations of these results. For column 6 and 7,

the standard error values obtained from fitting the linear trend are shown.

4 Results and discussions

Table 1 thus lists all the measured resistance values that were introduced. We used in total 4 bonding steps on each device to perform the subsequent measurements (in part because of a limited number of measurement wires in the setup). The order of the measurements was the following: (i) Column 2 and 3; (ii) Column 6; (iii) Column 4; (iv) Column 5 and 7.

The 2DEG resistance under the ohmic contacts is by about a factor 6 lower than the resistance of the pristine 2DEG (columns 2 and 3). This occurs for all annealing times. A previous study on ohmic contacts by [33] and our results [5] show that upon annealing Germanium diffuses from the surface towards 2DEG, and this increases n -doping near the 2DEG. While this can reduce the mobility in this region, the effective 2DEG square resistance apparently decrease due to the higher doping level. The resistance values are in the optimum lower limit for all the annealing times that we studied (20–350 s). This could suggest that Ge diffuses to 2DEG region already for short annealing times. Other studies also suggest that there is a range of annealing temperatures and times when the contact resistance almost remains constant [37].

Columns 4 to 7 in Table 1 show the contact resistance values as measured with different measurement schemes. The results show significant differences, that we can partly explain and which provide some insight in the different contributions to the contact resistance. As a starting point of the discussion we use the values in column 7, which is the TLM result for directly bonding on the ohmic contacts. Column 5 lists the contact resistance values measured with the 3-point method with bonding directly on the ohmic contact. Column 5 has values that are typically 3 Ω higher than the values in column 7. This can be explained by the fact that the result of column 5 contains a series resistance contribution from a 30 μm wide region of pristine 2DEG (from the distance between the ohmic contact and the 2DEG voltage probe, this 2DEG part is encircled in green in Fig. 5d). The expected resistance contribution of this part is indeed $\sim 3\Omega$ (using R_{\square} of column 2). This effect was also used for correcting the values of $R_{\square, \text{below}C}$ in column 3.

Table 2. The contact resistance values as measured by the TLM method (column 7 in Tab. 1) represented in various forms. Column 2 shows the measured value of the contact resistance. Columns 3, 4 and 5 show the same resistance values but converted to a value that is normalized to the contact width (column 3), a value for the specific contact resistance per contact area (column 4), and a bulk resistivity value for the material in the volume between the surface metallization and the 2DEG layer.

1	2	3	4	5
t_A (sec)	$R_{c,TLM-ohm}$ (Ω)	R'_c (Ωmm)	R_c (Ωcm^2)	ρ_{bulk} (Ωm)
20	0.41 ± 3.4	0.082 ± 0.68	$1.64 \times 10^{-4} \pm 1.36 \times 10^{-3}$	0.27 ± 2.26
50	1.24 ± 1.13	0.248 ± 0.226	$4.96 \times 10^{-4} \pm 4.52 \times 10^{-4}$	0.83 ± 0.75
100	2.38 ± 0.41	0.476 ± 0.82	$9.52 \times 10^{-4} \pm 1.64 \times 10^{-4}$	1.59 ± 0.27
350	2.30 ± 0.30	0.46 ± 0.06	$9.2 \times 10^{-4} \pm 1.2 \times 10^{-4}$	1.53 ± 0.2

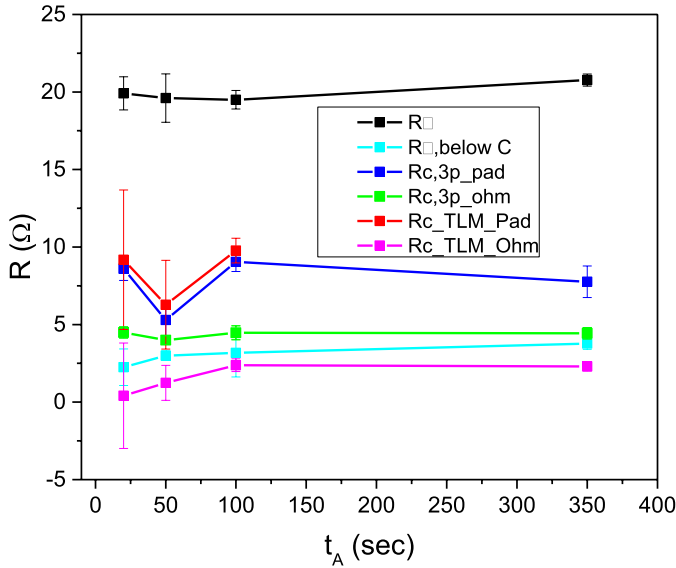


Fig. 6. All the measured resistance values that are given in Table 1 are plotted here. To make it convenient the legends and labels for the different resistance values are similar as used in Table 1.

Column 6 shows resistance values from the TLM method with bonding on the side pad (note that 2 side pads are involved) and these results are about $2 \times 3 \Omega$ higher than the values in column 7. Similarly, the results of column 4 (3-point, bonding on pad, note that only 1 side pad is involved) are about $1 \times 3 \Omega$ higher than the values in column 5 (3-point, bonding on ohmic). Here we must consider two possible explanations. The first is that the act of pressing a bond wire on top of the ohmic contact results in a lowering of the effective contact resistance by about 3Ω . The second possibility is that it results from the fact that the metal side pads are only connected to the surface metal of the ohmic-contact at one narrow point. This can yield that on average the spreading resistance inside the contact gives a contribution that is about 3Ω higher for the cases with bonding on the side pads. Given that all our measurement results and the various contributions are on the scale of only a few Ω , we can not distinguish these cases (we could rule out that it was due to series resistance inside the metal side pad and its inter-connect). The square resistance of 2DEG under the contacts stays the same within error bars with increasing

the annealing time (Cyan color in Fig. 6). Similarly the resistance of the ohmic contacts also remains the same for all the annealing times for the TLM data when wires are bonded on top of the ohmic contacts (magenta color in Fig. 6 and Columns 7 in Tab. 1). Due to the overall low resistance values of the contacts and 2DEG, we can not give a strong statement about the effect of 2DEG square resistance on the resistance of the contacts.

Our results do not allow for more detailed conclusions on the various contributions to the contact resistance or on the annealing mechanism. The reason is that the measured contact resistance values were all much lower than expected (given our earlier work [5]) and did not show considerable dependence on the annealing time. In addition, the possible effects of spreading resistance and small series-resistance contributions are all on the scale of a few Ω , and these values are close to the total contact resistance values and their statistical variation. This rules out that further analysis of our present results can give sufficient accuracy for answering the questions that we aimed to study.

At the same time, it is an interesting result that we find very low contact-resistance values, and that the values remain sufficiently low and constant within error bars when changing the annealing time by a factor 18. In addition, these contact resistance values are comparable to the lowest reported values [28] for the similar 2DEG systems. It is important to take into consideration the depth of the 2DEG, doping of the capping layer and the thickness of the buffer layer in order to compare the different 2DEG systems as they all play a role in determining the lowest contact resistance values. Table 2 provides different representations of the resistance values that we obtained. These values are useful for a comparison to values in the literature where authors present values of contact resistance in various ways. When comparing the literature one also needs to account for a dependence on the depth of the 2DEG and the thickness of the buffer layer. Our results on the wafer with the 2DEG at 180 nm depth (instead of 60 nm) show indeed slightly higher values, with for $R_{c,3p-pad} \approx 15 \Omega$. Also these samples showed almost no dependence on annealing time (similar results for 30 s and 550 s).

We have at this stage little insight why the fabrication method that we used gives such low and optimal contact-resistance values, while also being fairly robust against a variation in annealing time. We have some initial results

that point out that the variation of the heating profile as a function of time during annealing is important. For the experiments on the samples with the 2DEG at 180 nm depth we compared results of annealing for 550 and 600 s annealing times with 5 s RTA ramp time, to results for 550 s annealing time that started after a 120 s RTA ramp time (similar to the glass-tube oven). The samples of the latter batch had contact resistance values that were twice as high. A second important difference with our earlier work [5] is that the glass-tube oven heats the sample in a gas flow, while the RTA heats the sample by radiation. This can influence the exact way the surface metallization gets heated, and thereby have an influence on the annealing mechanism. Finally, there is possibly a role for having a suitable very clean N₂ flow during annealing, and a very clean sample surface before fabrication is started (samples that appeared dirty upon inspection did not yield results with low contact-resistance values).

We do not speculate which possible microscopic model of the ohmic contact forming could be the most appropriate one. Our present work shows that it is certain that the heterostructure right underneath the metallization is completely degenerated, either homogeneously [5] or in contact spikes [29,31]. In the first case, the contact conductivity should be proportional to the circumference length which we cannot check due to the fixed dimensions in this study. In the latter case of contact spikes it depends on their spacing: If they are closely packed, the circumference should again determine the conductivity. If they are more apart, the area could be the leading term. The transmission-electron-microscope studies of our earlier work [5] did rule out a role for spike formation. However, given the very different behavior of the annealing step we cannot conclude that this also holds for the present study.

5 Conclusions

We developed a dedicated device to study and unravel the various contributions to the resistance values of an ohmic contact. We could show that the 2DEG resistance under an ohmic contact gets lower upon annealing, and that pressing a bonding wire onto an ohmic contact either has little influence or only lowers it by a few Ω . The 2DEG square resistance underneath the contact is significantly lower than the pristine 2DEG square resistance. We could not fully exploit the measurement possibilities of our device design because we obtained very low contact-resistance values when annealing times were varied from 20 to 350 s. Our measurements show that these results can be obtained with rapid heating (5 s ramp time) during annealing, and that slower ramp times cause higher contact resistance values.

We thank B. Wolfs, J. Holstein and M. de Roos for technical assistance. A.D.W. acknowledges financial support from the DFG-TRR160, BMBF - Q.Link.X 16KIS0867, and the DFH/UFA CDFA-05-06. M.J.I. acknowledges a scholarship from the Higher Education Commission of Pakistan.

Author contribution statement

M.J.I performed the research work under the supervision of C.H.v.d.W. The manuscript was written by M.J.I and C.H.v.d.W. with contributions from D. R. and A.D. W. The 2DEG samples used in this research work were grown by D.R. and A.D.W.

References

1. C.W.J. Beenakker, H. van Houten, *Solid State Phys.* **44**, 1 (1991)
2. *Mesoscopic Electron Transport*, edited by L.L. Sohn, L.P. Kouwenhoven, G. Schön, NATO ASI Series E (Kluwer, Dordrecht, Netherlands, 1997), Vol. 345
3. A.G. Baca, F. Ren, J.C. Zolper, R.D. Briggs, S.J. Pearton, *Thin Solid Films* **308–309**, 599 (1997)
4. C. Salhani, J. Rastikian, C. Barraud, P. Lafarge, M.L. Della Rocca, *Phys. Rev. Appl.* **11**, 014050 (2018)
5. E.J. Koop, M.J. Iqbal, F. Limbach, M. Boute, B.J. van Wees, D. Reuter, A.D. Wieck, B.J. Kooi, C.H. van der Wal, *Semicond. Sci. Technol.* **28**, 025006 (2013)
6. M.J. Iqbal, Ph.D. thesis, *Electron Many-Body Effects in Quantum Point Contacts* (2012), <http://irs.uv.rug.nl/ppn/344115682>
7. M.J. Iqbal, R. Levy, E.J. Koop, J.B. Dekker, J.P. De Jong, J.H.M. van der Velde, D. Reuter, A.D. Wieck, R. Aguado, Y. Meir, C.H. van der Wal, *Nature* **501**, 79 (2013)
8. M.J. Iqbal, J.P. De Jong, D. Reuter, A.D. Wieck, C.H. van der Wal, *J. Appl. Phys.* **113**, 024507 (2013)
9. N. Braslau, J.B. Gunn, J.L. Staples, *Solid-State Electron.* **10**, 381 (1967)
10. M. Ogawa, *J. Appl. Phys.* **51**, 406 (1980)
11. N. Braslau, *J. Vacuum Sci. Technol.* **19**, 803 (1981)
12. C.P. Lee, B.M. Welch, J.L. Tandon, *Appl. Phys. Lett.* **39**, 556 (1981)
13. M. Heiblum, M.I. Nathan, C.A. Chang, *Solid-State Electron.* **25**, 185 (1982)
14. T.S. Kuan, P.E. Batson, T.N. Jackson, H. Rupprecht, E.L. Wilkie, *J. Appl. Phys.* **54**, 6952 (1983)
15. N. Braslau, *Thin Solid Films* **104**, 391 (1983)
16. N. Braslau, *J. Vacuum Sci. Technol. A* **4**, 3085 (1986)
17. M. Procop, B. Sandow, H. Raidt, L.D. Son, *Phys. Status Solidi A* **104**, 903 (1987)
18. J.R. Waldrop, R.W. Grant, *Appl. Phys. Lett.* **50**, 250 (1987)
19. R.A. Bruce, G.R. Piercy, *Solid-State Electron.* **30**, 729 (1987)
20. J.R. Shappirio, R.T. Lareau, R.A. Lux, J.J. Finnegan, D.D. Smith, L.S. Heath, M. Taysing-Lara, *J. Vacuum Sci. Technol. A* **5**, 1503 (1987)
21. E. Relling, A.P. Botha, *Appl. Surf. Sci.* **35**, 380 (1988)
22. V.G. Weizer, N.S. Fatemi, *J. Appl. Phys.* **64**, 4618 (1988)
23. N.E. Lumpkin, G.R. Lumpkin, K.S.A. Butcher, *J. Mater. Res.* **11**, 1244 (1996)
24. D. Taneja, F. Sfigakis, A.F. Croxall, K. Das Gupta, V. Narayan, J. Waldie1, I. Farrer, D.A. Ritchie, *Semicond. Sci. Technol.* **31**, 065013 (2016)
25. P. Zwicky, S.D. Mukherjee, P.M. Capani, H. Lee, H.T. Griem, L. Rathbun, J.D. Berry, W.L. Jones, L.F. Eastman, *J. Vacuum Sci. Technol. B* **4**, 476 (1986)
26. T.K. Higman, M.A. Emanuel, J.J. Coleman, S.J. Jeng, C.M. Wayman, *J. Appl. Phys.* **60**, 677 (1986)

27. A.K. Rai, A. Ezis, R.J. Graham, R. Sharma, D.W. Langer, *J. Appl. Phys.* **63**, 4723 (1988)
28. Y. Jin, *Solid-State Electron.* **34**, 117 (1991)
29. R.P. Taylor, P.T. Coleridge, M. Davies, Y. Feng, J.P. McCaffrey, P.A. Marshall, *J. Appl. Phys.* **76**, 7966 (1994)
30. A. Messica, U. Meirav, H. Shtrikman, *Thin Solid Films* **257**, 54 (1995)
31. R.P. Taylor, R. Newbury, A.S. Sachrajda, Y. Feng, P.T. Coleridge, M. Davies, J.P. McCaffrey, *Superlattices Microstruct.* **24**, 337 (1998)
32. S. Raiser, U. Graumann, M. Fleischer, J. Schmid, S. Jauerneck, J. Weis, D.A. Wharam, Scientific program of the 2005 German DPG meeting, abstract HL 58.67 (unpublished) see DPG FrÄ1/4hjahrstagung, Session HL58 entry 67 (HL 58.67 Di 16:30 Poster TU F) (2005), <http://www.dpg-tagungen.de/archive/>
33. G. Sai Saravanan, K. Mahadeva Bhat, K. Muraleedharan, H.P. Vyas, R. Muralidharan, A.P. Pathak, *Semicond. Sci. Technol.* **23**, 025019 (2008)
34. R.E. Williams, *Modern GaAs Processing Methods*, (Artech House Publishers, 1990)
35. H.H. Berger, *Solid-State Electron.* **15**, 145 (1972)
36. G.K. Reeves, H.B. Harrison, *IEEE Electron Device Lett.* **3**, 111 (1982)
37. V.I. Egorkin, V.E. Zemlyakov, A.V. Nezhentsev, V.I. Garmash, *Russian Microelectr.* **46**, 272 (2017)

Cite this article as: Muhammad Javaid Iqbal, Dirk Reuter, Andreas Dirk Wieck, Caspar van der Wal, Characterization of low-resistance ohmic contacts to a two-dimensional electron gas in a GaAs/AlGaAs heterostructure, *Eur. Phys. J. Appl. Phys.* **89**, 20101 (2020)